



Minerva Access is the Institutional Repository of The University of Melbourne

Author/s:

Akinoglu, GE;Quan, D;Rokhsat, E;Hutchison, JA

Title:

Tensile Control of Vibrational Strong Light-Matter Coupling with Flexible Polyester Films

Date:

2024-10

Citation:

Akinoglu, G. E., Quan, D., Rokhsat, E. & Hutchison, J. A. (2024). Tensile Control of Vibrational Strong Light-Matter Coupling with Flexible Polyester Films. *Advanced Functional Materials*, 34 (40), <https://doi.org/10.1002/adfm.202403657>.

Persistent Link:

<https://hdl.handle.net/11343/351020>

License:

[cc-by-nc](#)

Tensile Control of Vibrational Strong Light-Matter Coupling with Flexible Polyester Films

Goekalp Engin Akinoglu,* Dali Quan, Eliza Rokhsat, and James Andell Hutchison*

Polaritons are generated by strong interaction between photons and matter, with the hybridization fundamentally changing the energy landscape of the system. Future exploitation of polaritons will benefit from implementing low-cost, flexible, and easily tuneable configurations, as electronics have before. Here, coherent coupling of the carbonyl stretch vibrations of polyester (poly(ethylene terephthalate), PET) films to the optical modes of a Fabry–Perot (FP) cavity is presented, in which the FP cavity is directly formed on flexible, free-standing, and commercially available PET films. For 2- μm thick PET films, the carbonyl stretch vibration of the PET overlaps with the half-wavelength FP cavity mode, leading to the coupling of the two modes, a Rabi splitting above 160 cm^{-1} , and associated anticrossing in angular dispersion measurements. The study demonstrates dynamic control of light-matter interaction strength by modulating film thickness under tension, finding that a 25% tensile stretch can tune the light-matter interaction from 20:80 mixing to near-perfect 50:50 hybridization at normal incidence. These findings are discussed in the context of future foldable/twistable/wearable polaritonic devices.

field, allowed through the Heisenberg uncertainty principle. The potential to modify material properties via strong coupling to optical resonators has attracted tremendous interest in photochemistry,^[3,4] quantum computing,^[5,6] optoelectronics,^[7–9] long-range energy transfer,^[10] and spintronics.^[11]

The coupling strength depends on the field confinement within an optical cavity but is also influenced by the transition dipole moment of the material in question. Consequently, most systems explored thus far operate within the visible spectral range, where numerous materials exhibit high oscillator strength electronic transitions. Recently, vibrational strong coupling has emerged as a new tool to investigate the physico-chemical properties of polaritons.^[12] The first observations of vibrational strong light-matter coupling with polymethyl

methacrylate (PMMA) films were reported in 2014^[13] and 2015.^[14]

Here, we show that vibrational strong light-matter coupling can be realized with commercially available biaxially-oriented PET films, commonly known as BOPET and commercially as Mylar. These ultra-thin PET films, with thicknesses ranging from several hundred micrometers to below 1- μm thickness, are fabricated by stretching PET films in orthogonal directions. The process has a large throughput, allowing precise control of the final thickness. Due to its high tensile strength, chemical and dimensional stability, moisture impermeability, transparency, and electrical properties, PET is used for many applications.^[15] In 2013 alone, the annual production of PET was 56 million tonnes.^[16] The films are also extremely cheap and readily available, utilized in various applications such as food sealing, packaging, thermal insulation, and photography.

We demonstrate that Mylar films can be fabricated into free-standing and flexible Fabry-Perot optical cavities by directly depositing thin gold mirrors on both sides. Specific thicknesses of the PET/Au FP cavities show an explicit anticrossing between the FP cavity mode and C=O stretch vibrations of the carbonyl groups of the PET that is indicative of strong light-matter coupling. These angular dispersions are also shown to depend on the metal mirror thicknesses. Our findings thus reveal that vibrational polaritonic materials can be feasibly fabricated on a large

1. Introduction

Modulating material properties with hybrid light-matter states is a rapidly emerging field of research with potential in chemistry, photonics, and sensing.^[1] Strong light-matter coupling can occur when a photon is resonant with the transition energy of a material confined in an optical cavity, and energy exchange between them is faster than the decay of the photonic and material components alone. As a result, two new modes emerge: the lower and higher polariton. Contrary to intuition, strong coupling between molecules and light is possible without the presence of any applied photons.^[2] This is possible due to vacuum fluctuations, the finite zero-point energy of an optical

G. E. Akinoglu, D. Quan, E. Rokhsat, J. A. Hutchison
ARC Centre of Excellence in Exciton Science
School of Chemistry
University of Melbourne
Parkville, VIC 3010, Australia
E-mail: engina@zedat.fu-berlin.de; james.hutchison@unimelb.edu.au

The ORCID identification number(s) for the author(s) of this article can be found under <https://doi.org/10.1002/adfm.202403657>

© 2024 The Authors. Advanced Functional Materials published by Wiley-VCH GmbH. This is an open access article under the terms of the Creative Commons Attribution-NonCommercial License, which permits use, distribution and reproduction in any medium, provided the original work is properly cited and is not used for commercial purposes.

DOI: 10.1002/adfm.202403657

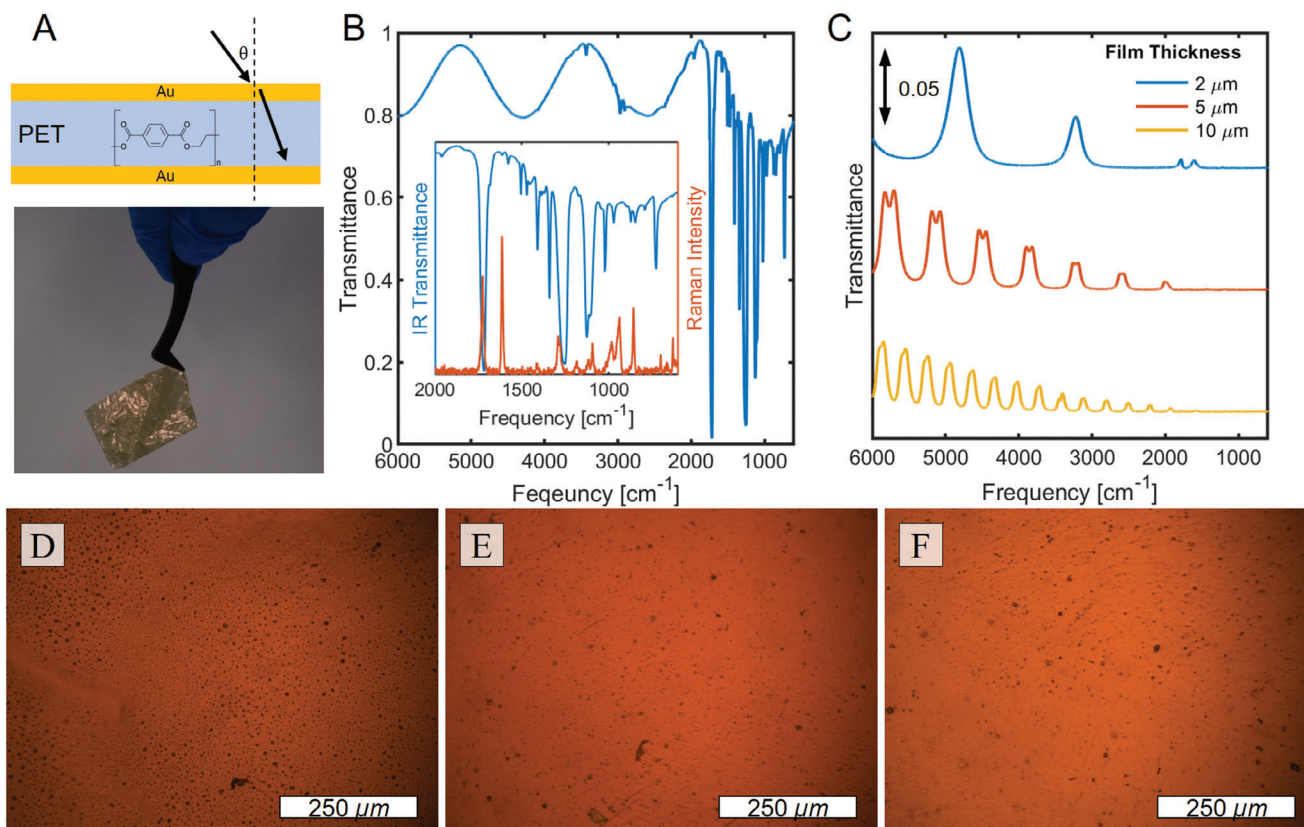


Figure 1. Double-side gold-coated PET films. A) Schematic and photograph of gold-coated PET films; B) IR transmittance and Raman spectra of PET without gold and C) 10 nm gold-coated PET films with different thicknesses as indicated; D–F) Optical brightfield images of 10 nm gold-coated PET films on D) 2-, E) 5-, and F) 10- μm thick PET. Despite many defects, the FP resonator modes have good Q-factors (15–30).

scale. Additionally, we demonstrate that the formation of polaritons can be adaptively adjusted with tensile tuning of the cavity thickness.

Dynamic tuning of polariton composition (light:matter mixing ratio) has found increasing interest due to its potential to engineer the function of polariton-based devices. Previous research has, for example, demonstrated photo-modulation of the material oscillator strength (optical control of a photochromic equilibrium^[20]) or electrical modulation of the resonance condition (electrical gating to shift the bandgap of 2D materials^[17,18]). Alternatively, gold-coated atomic force microscopy (AFM) tips can modify the interaction between light and 2D materials by adjusting the mode volume and near-field polarization. They can also apply pressure, influencing strain, bandgap, and emissivity.^[19] Here, we extend these existing works of dynamically tunable exciton-polaritons to vibration-based polaritons in the mid-infrared. The flexible and plastic nature of our free-standing PET FP cavities allows for tensile stretch-tuning of the cavity thickness and, thus also, light-matter interaction strength. We show that the cavities can be stretched by up to 25% without physical failure, with tolerable degradation of the optical cavity quality (Q-)factor. However, this degree of stretching can take the system from the weak to the strong coupling regime for a fixed angle, which may have consequences when considering future foldable, twistable, and wearable devices that utilize polariton resonances.

2. Results and Discussion

Free-standing FP cavities were fabricated by sputtering gold directly on Mylar films. While sputtering is a versatile and widely used technique for depositing thin films over large areas, it can introduce damage to underlying soft/organic films due to the high-energy particle bombardment inherent in the process. This contrasts with other vacuum-based deposition techniques (e.g., thermal and e-beam), which may operate under conditions less likely to induce such damage, making them more suitable for sensitive substrates. This issue can be mitigated by introducing a protective layer, a solution typically employed during solar cell fabrication.^[20] An alternative method involves initially depositing metal onto a sacrificial layer, then transferring this metal onto the target surface, followed by the removal of the sacrificial layer.^[21] However, as seen in **Figure 1A**, the directly sputter-coated Mylar films herein are highly stable without any support structure and exhibit luster suggestive of optically smooth surfaces (vide infra).

Figure 1B shows the Fourier transform infrared (FTIR) transmission spectrum of a $\approx 2 \mu\text{m}$ -thick PET film without metal coating. The spectrum already shows broad oscillations, which are the manifestation of FP interferences due to the reflections at the air/polymer interface. For energies lower than 2000 wavenumbers, many absorption bands appear, caused by the excitation of molecular vibrations of the PET, which is also verified with Raman measurements. However, the interference effects for the

neat PET film are extremely lossy because the reflection coefficient at the polymer-air interface is small (<5%). The consequence is a broadening of the FP resonances (reduced Q-factor). With the deposition of 10 nm gold mirrors on both sides of the PET films, the transmission through the FP cavity is significantly reduced, and the FP resonances can be observed as transmission peaks. Many modes appear, corresponding to the standing waves inside the cavity whose resonance energy can be tuned by the chosen film thickness (see Figure 1C). The thickness can be estimated approximately using the free spectral range, as detailed in the Supporting Information.

In addition, the Q-factor of the FP resonances with the 10 nm gold mirrors is greatly enhanced as light is better contained inside the cavity. For the 2- μm cavities, we observe a Q-factor of ≈ 15 ; for 5- μm cavities, Q-factors of ≈ 20 ; and for 10- μm cavities, the quality factors increase to ≈ 30 . We attribute the lower quality factor for thinner cavities to inhomogeneous angular broadening. As seen in Figure 1A, the 2- μm film is slightly wrinkled, leading to angular dispersion of transmission (vide infra), but it flattens for thicker films. Nevertheless, the Q-factors of the FP cavities are still in the same order of magnitude as those used for reaching vibrational strong light-matter coupling, as reported in the literature, with Q-factors up to 60.^[12] This is astounding as the PET films are industrial grade and show many defects on a macroscopic level, as seen in the optical micrographs in Figure 1D–F. The optical beam width of a typical FTIR spectrometer spans several square centimeters so that all these imperfections are averaged over during the measurement.

The resonance energy of the FP modes can be calculated as follows:^[22]

$$E_c(k_{\parallel}) = \frac{hc}{n_c} \sqrt{\left(\frac{m\pi}{L_{\text{cav}}}\right)^2 + k_{\parallel}^2} \quad (1)$$

where m is the mode order, n_c is the refractive index inside the cavity, and L_{cav} is the thickness (mirror-to-mirror separation) of the FP cavity. The in-plane wavevector k_{\parallel} is dependent on the wavelength and the angle of incidence θ through:

$$k_{\parallel} = \frac{2\pi}{\lambda} \sin\theta \quad (2)$$

Thus, the optical modes show strong angular dispersion, whereas material excitations are wavevector independent. For a film thickness of 2 μm and a dispersionless refractive index of $n = 1.5$ for PET, Equation (1) gives resonance energies of 5000 cm^{-1} ($m = 3$), 3333 cm^{-1} for ($m = 2$), and 1666 cm^{-1} ($m = 1$) at normal incidence. These estimates are slightly larger than the experimental values in Figure 1C of 4808 cm^{-1} for the third and 3217 cm^{-1} for the second-order resonance (which is not interfered with by any interaction with PET vibrational modes), indicating that the manufacturer information might slightly deviate from the actual value. Careful comparison with transfer matrix simulations (Figure 2A), alongside analytical analysis, suggests that the exact thickness of the nominally 2-micron thick film is $\approx 1.91 \mu\text{m}$. This represents a relative deviation of less than 5%.

A double FP resonance is observed for all the optical modes in the 5- μm cavity and slightly less pronounced for the 10- μm cavity spectra. In the case of the 5- μm cavity, such a double FP reso-

nance could be due to the existence of two spatial domains with a $\approx 92 \text{ nm}$ difference in thickness. However, such a two-valued thickness distribution is not supported by topography measurements (vide infra). Instead, we attribute this effect to a birefringence introduced by uneven biaxial stretching during the Mylar manufacturing process. The alignment of polymer chains in specific orientations induces an anisotropy in the refractive index and creates a phase shift among diverging light paths.^[23] The double resonance can be removed by slightly stretching the PET films in specific directions or by using polarization filters (see Figure S1, Supporting Information).

For the 2- μm cavity, double FP resonances are not observed for any energy. However, a large doublet is observed at 1782 and 1602 cm^{-1} wavenumbers. This can be interpreted as the hybridization of the optical mode of the FP cavity to a vibrational mode of the PET. Figure 2B,C show the observed polaritonic peak splitting for the 2- μm cavity in more detail. The vibrational mode with the strongest transition dipole moment of PET is the C=O stretch vibration of the carbonyl groups, with absorption at 1718 cm^{-1} and a full width of half maximum (FWHM) of 35 cm^{-1} (Figure S2, Supporting Information), which can interact with the fundamental cavity mode at $\approx 1666 \text{ cm}^{-1}$ according to Equation (1). Indeed, we attribute this peak splitting to the coupling of the C=O stretch vibration to the optical mode, noting that the carbonyl absorption maximum of the uncoupled PET is located at the transmission minimum of the cavity spectrum. This interaction occurs despite a mismatch of $\approx 60 \text{ cm}^{-1}$ between the first-order optical mode and the C=O stretch vibration at normal incidence. These polaritonic branches will be examined in more detail further on.

Raman measurements of the PET films and cavities were also taken (Figure 1B inset and Figure 2B respectively). Early studies by Shalabney et al.^[24] suggested that the Rabi splitting of the C=O stretch vibration of polyvinyl acetate coupled to an optical mode can be measured with Raman spectroscopy. However, subsequent studies indicated that the peak assigned to the polariton formation is an effect of polymer degradation during Raman measurements.^[25] Work on other systems also suggests that Raman spectroscopy cannot resolve the polariton formation of vibrational modes.^[26] We do not observe a peak splitting of the C=O stretch Raman signal for the 2- μm cavity (Figure 2B). The Raman band at 1614 cm^{-1} , which is resonant with the lower polariton, is assigned to the 8a ring mode of the PET benzene ring and is also observed for the PET without gold-coated mirrors (Figure 1B inset).^[27] That Raman spectroscopy cannot resolve the polariton formation of vibrational modes has been attributed to the fact that Raman probes the entire assembly of vibrational oscillators, not just a fraction with transition dipole moments with significant components parallel to the cavity electric field.^[26] We note here that the 8a ring mode at 1614 cm^{-1} , which is resonant with the lower polariton in the 2- μm cavity, is relatively enhanced compared to the PET film. The Raman measurements feature a background signal reminiscent of surface-enhanced Raman (SERS) spectroscopy background signals (Figure S3, Supporting Information),^[28] which correlates with the Au film thickness and might be an effect of higher order FP modes matching with the laser excitation wavelength.

We investigated the effect of gold mirror thickness on the Q-factor and effective thickness of the 2- μm cavity, both

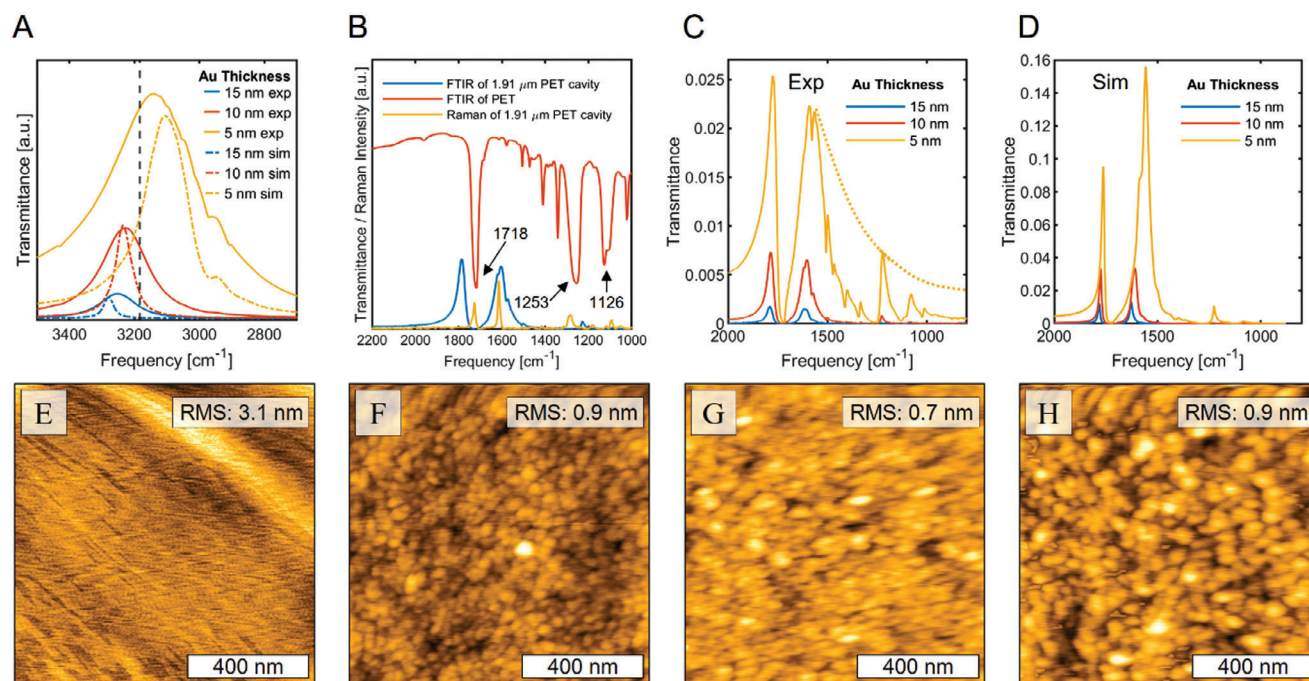


Figure 2. Strong light-matter coupling of 1.91 μm -thick FP cavity with the C=O stretch vibrations of the carbonyl groups of PET. A) Comparison of experimental and transfer matrix simulation of the $\approx 3200\text{ cm}^{-1}$ optical cavity mode as a function of metal thickness. The black dotted line represents the analytical solution at normal incidence based on Equation (1). B) FTIR and Raman spectra with and without 10 nm Au mirrors (The spectra are arbitrarily scaled for clarity). The splitting of the cavity transmission around the 1718 cm^{-1} C=O PET absorption is indicative of strong light-matter. C) Experimental transmission spectra of the cavity for different metal film thicknesses, peak splitting around the PET C=O stretch in each case. The dotted yellow line is a guide to the eye for the linewidth of the lower polariton peak without the interference of the other PET vibrational modes for a 5 nm gold coating. D) Simulated transmission spectra for the cavity with different metal film thicknesses. E–H) AFM images of Mylar films. E) Mylars without any Au coating, F) with 5 nm Au coating, G) with 10 nm Au coating, and H) with 15 nm Au coating.

experimentally and with transfer matrix simulations in Figure 2A, focusing on the optical mode at $\approx 3200\text{ cm}^{-1}$ that is not strongly perturbed by interactions with PET vibrational modes. As the gold mirror thickness increases, the Q-factor increases, as discussed earlier; however, the effective thickness of the cavity reduces (the mode blue shifts). This blue shift is progressively greater than predicted by simulation as gold thickness increases, suggesting that it is due to better confinement of the optical modes but also because of the penetration of the gold into the film as more is deposited.

Next, we investigated the effect of mirror metal thickness on the polariton resonances. As seen in Figure 2C for experiments and in Figure 2D for simulations, the metal thickness has a negligible effect on the polariton spectral position, where the lower polariton redshifts from 1614 cm^{-1} (5 nm Au) to 1575 cm^{-1} (15 nm Au). However, smaller metal thicknesses increase the overall (off-resonance) transmission from de facto zero for 10 nm mirror thicknesses to 0.4% for 5 nm metal thicknesses. In addition, we observe an absolute broadening of the lower and upper polariton for smaller metal thicknesses. The Q-factor of the optical modes reduces from 20 for 15 nm mirror thicknesses down to 9 for 5 nm thick mirrors. The broadening becomes significant for 5 nm thickness, such that the lower polariton peak overlaps with most of the other vibrational modes of PET. As the polariton manifests itself in a transmission peak compared to the baseline, most of the vibrations of PET can then be resolved. In fact, the lower polariton is much broader than at first glance. For example,

the peak at 1220 cm^{-1} , higher than the baseline values at high frequencies, is a consequence of the transparency window between the vibrational absorption band at 1253 and 1128 cm^{-1} . Thus, while the Q-factor is significantly reduced, it is remarkable that 5 nm Au is enough to form a practical mirror for the FP cavities.

Atomic force microscopy (AFM) images confirm that the Mylar films are flat with a root mean square (RMS) roughness of 3.1 nm (Figure 2E). After gold deposition, the surface roughness actually improves, down to 0.7 nm (Figure 2F–H). Ultra-thin metal films vacuum-deposited on rigid substrates like silicon tend to de-wet and form island-like structures that can be plasmonically active and are used for surface-enhanced Raman^[29] and IR spectroscopy.^[30] Such films generally only form continuous layers for thicknesses above 15 nm.^[29] Gold film thicknesses $>15\text{ nm}$ drastically reduce transmission and, hence, the coupling of the light into the FP cavity. This is especially so in the infrared, where metal films are close to perfect conductors and penetration depths are lower than in the visible.^[31] Therefore, the smooth and surface-wetted $<15\text{ nm}$ sputtered films of Au on PET obtained here are highly advantageous.

In addition, we note that the 5 nm Au films, in which all the PET vibrational modes can be identified, as well as the polariton modes, may have other advantages. They may allow, for example, the in-situ monitoring of reaction kinetics in polariton chemistry experiments. Such experiments are performed in microfluidic cells, and the reaction products are generally analyzed outside of the cell with nuclear magnetic resonance spectroscopy,^[32] gas

chromatography-mass spectroscopy,^[33] or even scanning electron microscopy.^[34] However, the ex situ characterization of production yields is susceptible to systematic errors, such as quantity lost during transfer or the precise determination of the reaction time. Hence, in situ measurements inside the reaction cell are crucially important considering current challenges in reproducing the change of reaction kinetics for polariton chemistry, as reported in Ref. [35] As such, achieving vibrational strong coupling with ultra-thin metal mirrors that allow simultaneous monitoring of all the vibrational modes is highly desirable. Counting against this, of course, is the reduction in cavity Q-factor, which may bring the system out of the strong light-matter interaction regime, but some balance may be found.

We next return to and analyze in detail the spectral splitting observed ≈ 1718 cm⁻¹ in the 2- μ m cavity, attributed to the strong coupling of a cavity optical mode and the PET C=O stretch. An essential characteristic of strong light-matter coupling is a distinct anti-crossing behavior, observed as the optical mode is scanned through the molecular transition energy resonance, either by angle- or thickness-tuning of the optical cavity (see Equations 1 and 2). The resonance condition occurs when the two new eigenstates for the system, the lower and upper polariton, approach closest in energy. At this condition, the splitting energy (Rabi splitting) should be greater than the widths of the composite material and photonic modes to affirm strong light-matter coupling (the frequency domain equivalent of the energy exchange between the cavity photonic mode and the material absorber being faster than any decay processes). The new polariton branches should inherit a partially dispersive nature from their photonic component.

Figure 3A–C depicts the experimental angular dispersions of transmittance for the 2- μ m cavity, with different metal thicknesses, and at 5-degree intervals. The dotted white line represents the absorption energy of the uncoupled C=O mode in each case. The lower polariton asymptotically approaches the C=O absorption line for large angles while the upper polariton diverges. No crossing between the lower and upper polariton is observed. There is an excellent agreement between experimental and computational simulations, as seen in **Figure 3D–F**. The simulations were conducted with a resolution of one degree. The solid white line indicates the dispersion of the uncoupled cavity mode derived from the simulations of the same cavity containing a flat 1.5 refractive index material without the C=O stretch. We observe a different anti-crossing point for the different mirror thicknesses. The highest anti-crossing occurs with mirrors with a thickness of 5 nm at 42 degrees, which is then reduced to 34 degrees for the 15 nm thick mirrors. Hence, while tuning the cavity length or the incident angle can be used to adjust the resonance energy of the FP, it is also feasible to alter the excitation energy of the polariton resonances by the mirror thickness to some degree. Further, we observe that the computed polariton's linewidth is slightly smaller than the experimental one. We attribute this observation to the multiple defects, as seen in the optical measurements (**Figure 1E**), and to the inhomogeneous angular broadening due to macroscopic wrinkling of the free-standing PET films, as mentioned earlier (**Figure 1A**).

Additionally, we plot the difference between upper and lower polariton as a function of angle, both experimentally (**Figure 3G**) and from simulations (**Figure 3H**). The experimental polariton

peak positions were determined by a constrained Gaussian fit. The experimental branch splitting exhibits angular trends that mirror those found in the computational analyses. However, the experimental data reveal marginally greater branch splitting, which we attribute to the broader FWHM of the experimental polaritons (**Figure 3I**), slightly distorting the derived values.

The vacuum Rabi splitting is defined as the point of the anti-crossing, where the branch splitting has a local minimum.^[13] However, we only observe a clear increase in peak splitting when tuning to higher angles. Tuning toward smaller angles flattens the branch splitting, especially in the case of 15 and 10 nm mirror thickness cavities. Further, we do not observe a clear local minimum for small initial detuning energies between the optical cavity and C=O stretch vibration as observed for 15 nm Au thickness.

Nevertheless, we can compare the Rabi splitting at resonance for each case with the widths of C=O stretch and the optical cavity mode for each mirror thickness. The derived Rabi frequencies of ≈ 160 cm⁻¹ or 19.8 meV for the 10 and 15 nm gold mirror cavities are comparable to those observed in similar FP cavities with other polymers with carbonyl groups, such as polymethyl methacrylate (PMMA)^[14] and polyvinyl acetate (PVAc).^[13] Such a large Rabi splitting is a consequence of the collective coupling of the vibrational modes. The vacuum Rabi splitting is proportional to the square root of the number of oscillators, expressed as $\Omega_R = \Omega \sqrt{N}$. Although the oscillator strength of each individual C=O stretch vibration is weak, the coherent coupling is amplified by the high number of oscillators, achieving an effective concentration of up to 3.64×10^{21} cm⁻³.

Finally, we conducted tensile-stretching experiments to tune the 2- μ m FP cavity thickness, and thus its optical resonances, for dynamic control over light-matter interaction strength. Experiments were performed with a new batch of commercial samples with slightly different thicknesses than the previous films (see **Figure S4**, Supporting Information). The film thickness was determined by matching the experimentally observed second FP mode ≈ 3200 cm⁻¹ with the simulations. Films were axially stretched in $\approx 5\%$ intervals at a temperature of 90 °C, slightly above the glass transition temperature of PET. Due to molecular alignment and structural changes under tension, the film width becomes thinner in orthogonal directions to the stretch direction. We measured a Poisson ratio of ≈ 0.33 , which is closely aligned with the values reported in the literature.^[36]

The experimental angular dispersions of transmission of the 2- μ m cavity with 15 nm gold mirrors, with various degrees of tensile stretching, are shown in **Figure 4A–F**. The initial thickness of the films was 1985 nm, and the most stretched film (25% stretched) was 1865 nm thick. The black dotted lines correspond to the simulated polariton modes and the white line to the uncoupled FP mode (for a flat 1.5 refractive index material), while the white dotted line represents the C=O stretch vibration frequency. There is excellent agreement between the experimental results and the computational derived values. As stretching increases, the FP modes blue shift, and the anti-crossing point occurs at lower angles. Intriguingly, despite the substantial shift observed in the simulated FP mode in the absence of C=O absorption, the polaritonic branch energy shifts are notably less pronounced.

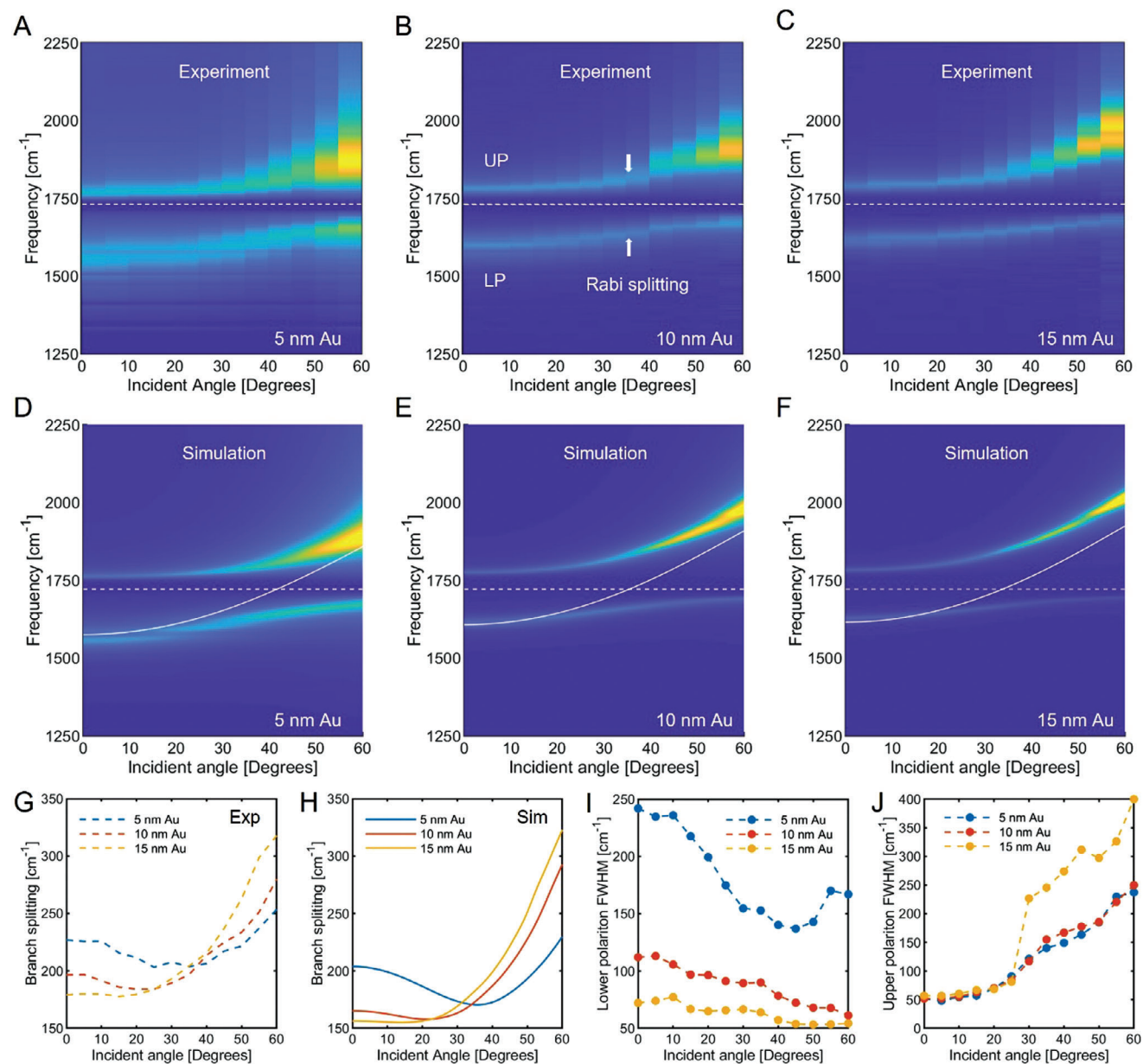


Figure 3. Angular dispersion of transmittance spectra for a 1.91 μm thick PET cavity with different metal thicknesses. The dotted line represents the absorption of the uncoupled C=O stretch vibration of PET, and the solid white line represents the dispersion of the calculated uncoupled cavity mode (in the absence of a C=O stretch). An anticrossing of the two modes can be observed in each case. A–C) Experiments and D–F) simulations. (A) and (D) 5 nm mirror thickness; (B) and (E) 10 nm mirror thickness; and (C) and (F) 15 nm mirror thickness. G) The experimental branch splitting energy and H) simulated branch splitting energy, showing good agreement. I) Experimental FWHM of the upper polariton, J) Experimental FWHM of the lower polariton.

Nevertheless, a careful examination at normal incidence reveals distinct dispersions of both the upper and lower polariton branches with increased stretching (Figure 4G). The reduced film thickness leads to a blue shift of the polariton resonances and a change in the light-matter coupling strength at a fixed angle. The lower polariton shifts from 1593 to 1639 cm⁻¹, and the upper polariton from 1777 to 1817 cm⁻¹. Further, we plotted the experimental (Figure 4H) and simulated (Figure 4I) polariton branch splitting as a function of angle. The experiments and predictions agree well, showing that the angle of minimum splitting (reso-

nance) reduces from 33 degrees to almost normal incidence upon stretching by 25% (Figure 4J).

The lower and upper polaritonic branches correspond to molecular vibrations dressed by the cavity vacuum field. The level of mixing between matter and light depends on the overlap between the optical resonance and the material's excitation. We used a coupled oscillator model (See Supporting Information for more details) to quantify the degree of mixing (Figure 5). The model assumes a collective coupling strength that reduces the interaction Hamiltonian to a 2 × 2 matrix.^[37] For the initial

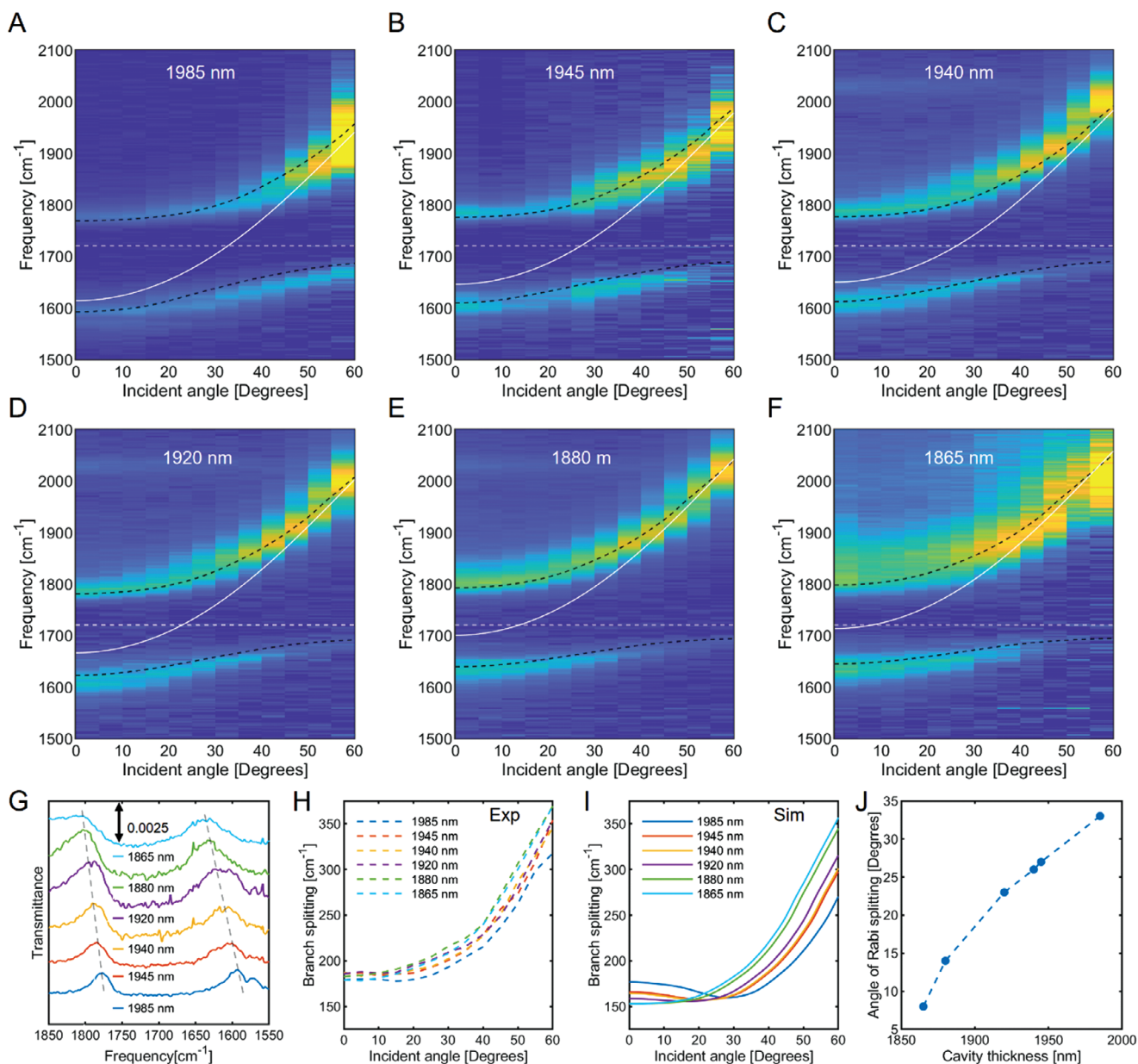


Figure 4. Tensile stretch-tuning of vibrational strong light-matter coupling. The 1.91 μm -thick PET cavities (15 nm gold mirrors) were stretched in $\approx 5\%$ intervals. Angular dispersive transmittance spectra with A) 1985 nm thickness B) 5% stretch and 1945 nm thickness, C) 10% 1940 nm thickness, D) 15% and 1920 nm thickness, E) 20% and 1880 nm thickness, and F) 25% stretch and 1865 nm thickness. The white dotted line represents the absorption of the uncoupled C=O stretch vibration of PET, the solid white line represents the dispersion of the simulated uncoupled cavity mode in the absence of C=O absorption, and the black dotted lines represent the simulated polaritonic modes for the PET cavity. G) Branch splitting at normal incidence for differently stretched films (polariton dispersion as a function of film thickness). H) Experimental branch splitting energy, I) Simulated branch splitting as a function of angle for each cavity thickness, J) Angle of anticrossing/resonance as a function of cavity thickness.

(unstretched) cavity thickness of 1985 nm, the composition of the C=O stretch vibration and FP cavity mode varies with angle, with 80:20 mixing across the two polariton modes at normal incidence. The upper polariton predominantly comprises the C=O vibration, whereas the lower polariton is primarily light. Going to higher angles, perfect hybridization (50:50 mixing) occurs at the anticrossing point, before the modes transition to either \sim entirely photonic (upper polariton) or \sim entirely matter (lower polariton), for larger angles. For reduced film thicknesses, as ten-

sile stretching is increased, the resonance point shifts to lower angles, until for a film thickness of 1865 nm (25% stretching), the 50–50 mixing condition occurs at near-normal incidence.

The observed Q-factor exhibits a progressive decline from 20 in the unstretched film to 8 for 25% stretching, as illustrated in Figure S5 (Supporting Information). For the realization of strong coupling, it is imperative that the Rabi splitting exceeds the combined dissipation losses of the FP cavity and the material's excitation mechanisms, where the losses can be determined by the

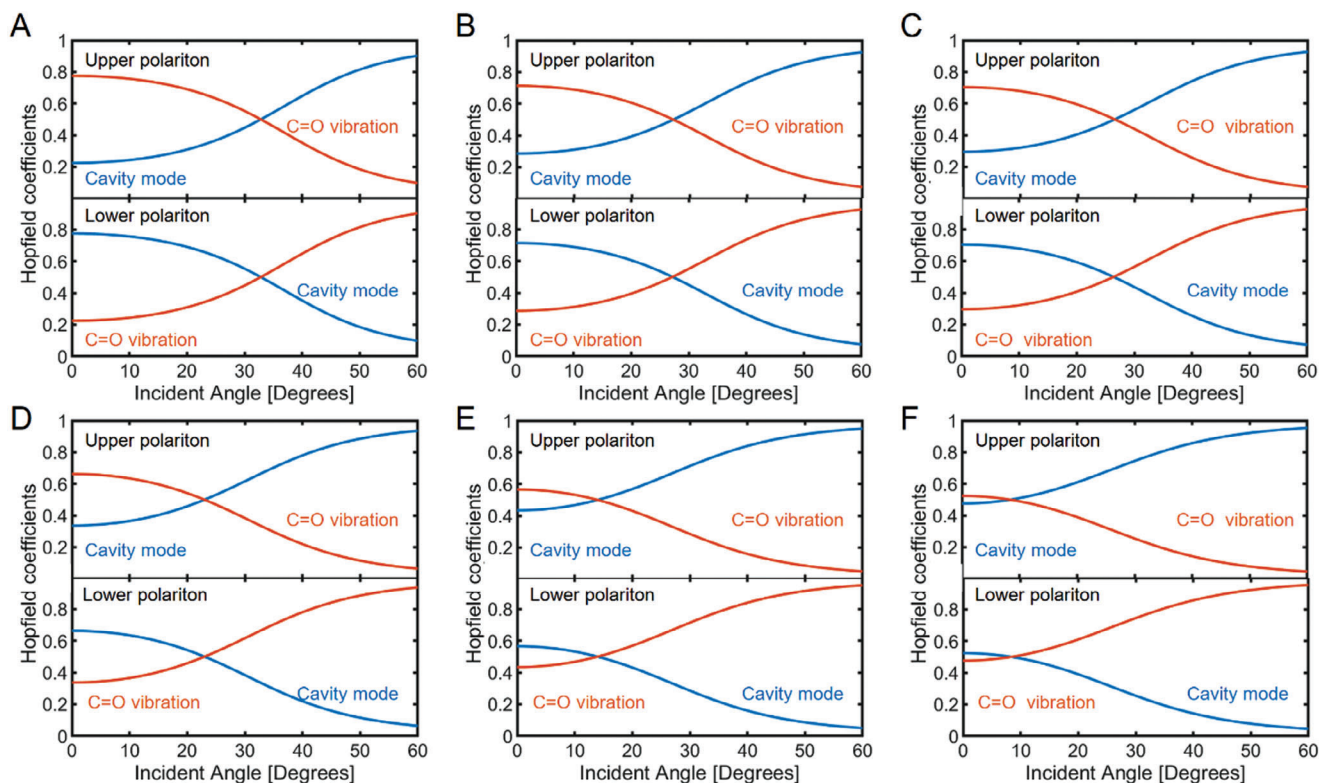


Figure 5. Eigenvector decomposition (Hopfield coefficients) for upper polariton and lower polariton branches derived from a coupled harmonic oscillator model analysis, for a 1.91 μm -thick cavity with 10 nm gold mirrors. With increasing stretching and reduction of cavity thickness, the mixing between the C=O stretch vibration and cavity mode for each branch shifts, approaching perfect 50:50 mixing at normal incidence for maximum stretching (25%). Calculated for cavity thicknesses of A) 1985 nm, B) 1945 nm, C) 1940 nm, D) 1920 nm, E) 1880 nm and F) 1865 nm.

FWHM of the resonances. $\Omega_R > \frac{\Delta\omega_{FP} + \Delta\omega_{PET}}{2}$. The FWHM of the C=O stretch vibration is 35 cm^{-1} , and the FWHM of the FP optical modes can be derived from the calculated quality factors. Due to the large Rabi oscillation, the system remains in a strongly coupled configuration despite an increased linewidth of the cavity modes.

These findings show that tensile stretching of free-standing, flexible FP-type optical cavities can dramatically affect the degree of vibrational light-matter coupling observed. In this case, a 25% tensile stretch can tune the light-matter interaction from 20:80 mixing to near-perfect 50:50 hybridization at normal incidence. On one hand, these free-standing, flexible PET optical cavities are cheap, large areas, and convenient materials to study vibrational strong coupling as a function of interaction strength in various contexts not possible with conventional rigid systems. On the other hand, these findings are worth considering in the context of the push toward flexible (opto)electronic devices. In the case of organic electronics, flexible devices must be able to maintain local interactions (e.g., free carrier hopping, exciton diffusion) as a material is stretched, folded, twisted, and so on. In the case of organic polaritonics, the challenge may be amplified. Not only must local material interactions be maintained, but a constant light-matter interaction strength may also need to be maintained, when even 25% stretching, quite typical in the context of wearable fabrics during human activity, (de)tune optical resonances drastically.

3. Conclusion

Vibrational strong light-matter coupling was achieved with free-standing, commercially available, biaxially-oriented PET film cavities coated with different metal thicknesses. The PET films have a root mean square roughness of 3.1 nm, reducing to $<1\text{ nm}$ roughness after gold mirror deposition. For PET films with $\approx 2\text{ }\mu\text{m}$ thickness, the half wavelength FP cavity mode couples to the stretch vibration of the carbonyl groups of the PET. At resonance, light-matter hybridization leads to a Rabi splitting above 160 cm^{-1} for optimized cavities. Finally, we demonstrated mechanical control of light-matter mixing by stretching the PET film cavities by up to 25%. This shifted the anti-crossing/resonance condition from an angle of 33 degrees to an almost normal incidence. At a fixed angle (normal incidence), the stretch-induced cavity thickness changes resulted in the light-matter mixing ratio changing from 80:20 to 50:50.

4. Experimental Section

Transfer matrix simulations were performed with MATLAB R2022b with a script kindly provided by Dr T. Chervy and Prof. Tal Schwartz. The refractive index of Au was taken from Ref. [38] and that from PET from Ref. [39]

Mylar PET films with different thicknesses were purchased from MicroWings (Caloundra DC, Queensland 4551, Australia). Gold was deposited with a Quorum Q150T S sputter coater in an argon atmosphere.

IR spectra were taken with a Bruker TENSOR 27 FTIR spectrometer with a resolution of 2 cm^{-1} . 24–128 accumulations were taken for each spectrum. Raman spectra were taken with a Renishaw Raman microscope equipped with a 633 nm laser. The integration time was set to 5 s, and 15 accumulations were taken for each spectrum.

Supporting Information

Supporting Information is available from the Wiley Online Library or from the author.

Acknowledgements

This work was partly performed at the Materials Characterisation and Fabrication Platform (MCFP) at the University of Melbourne and the Victorian Node of the Australian National Fabrication Facility (ANFF). The authors thank funding from the Australian Government through the Centre of Excellence in Exciton Science (CE170100026) and Discovery Project (DP160102754) and thank funding from the ANFF-Vic Technology Fellow Ambassador Program and the MCFP Sustainability Research Grant. J.A.H. thanks the Australian Government for funding through the Australian Research Council Future Fellowship scheme (FT180100295) and G.E.A. thanks funding through the Australian Government Research Training Program (RTP) Scholarship program.

Open access publishing facilitated by The University of Melbourne, as part of the Wiley - The University of Melbourne agreement via the Council of Australian University Librarians.

Conflict of Interest

The authors declare no conflict of interest.

Data Availability Statement

The data that support the findings of this study are available from the corresponding author upon reasonable request.

Keywords

dynamic control, Fabry–Pérot cavity, functional materials, mylar, rabi splitting, thin films, vibrational strong coupling

Received: February 29, 2024

Revised: April 16, 2024

Published online: May 1, 2024

- [1] D. S. Dovzhenko, S. V. Ryabchuk, Y. P. Rakovich, I. R. Nabiev, *Nanoscale* **2018**, *10*, 3589.
- [2] F. J. Garcia-Vidal, C. Ciuti, T. W. Ebbesen, *Science* **2021**, *373*, eabd0336.
- [3] R. Bhuyan, J. Mony, O. Kotov, G. W. Castellanos, J. Gómez Rivas, T. O. Shegai, K. Börjesson, *Chem. Rev.* **2023**, *123*, 10877.
- [4] M. Ruggenthaler, D. Sidler, A. Rubio, *Chem. Rev.* **2023**, *123*, 11191.
- [5] Z. Yang, W. Xiong, *Adv. Quant. Technol.* **2022**, *5*, 2100163.
- [6] A. Kavokin, T. C. H. Liew, C. Schneider, P. G. Lagoudakis, S. Klemmt, S. Hoefling, *Nat. Rev. Phys.* **2022**, *4*, 435.
- [7] M. A. Masharin, A. K. Samusev, A. A. Bogdanov, I. V. Iorsh, H. V. Demir, S. V. Makarov, *Adv. Funct. Mater.* **2023**, *33*, 2215007.
- [8] B. Zhang, Y. Li, X. Wu, X. Xu, Y. Lu, Q. Wu, X. Wang, H. Lei, J. Ma, G. Liao, Y. Li, *Laser Photonics Rev.* **2023**, *18*, 2300895.
- [9] H. Hu, N. Chen, H. Teng, R. Yu, M. Xue, K. Chen, Y. Xiao, Y. Qu, D. Hu, Q. Dai, *Science* **2023**, *379*, 558.
- [10] D. J. Tibben, G. O. Bonin, I. Cho, G. Lakhwani, J. Hutchison, D. E. Gómez, *Chem. Rev.* **2023**, *123*, 8044.
- [11] S. Liu, I. A. Malik, V. L. Zhang, T. Yu, *Adv. Mater.* **2023**, 2306920.
- [12] K. Nagarajan, A. Thomas, T. W. Ebbesen, *J. Am. Chem. Soc.* **2021**, *143*, 16877.
- [13] A. Shalabney, J. George, J. Hutchison, G. Pupillo, C. Genet, T. W. Ebbesen, *Nat. Commun.* **2015**, *6*, 5981.
- [14] J. P. Long, B. S. Simpkins, *ACS Photonics* **2015**, *2*, 130.
- [15] M. T. Demeuse, *Biaxial Stretching of Film: Principles and Applications*, Elsevier, Amsterdam **2011**.
- [16] S. Yoshida, K. Hiraga, T. Takehana, I. Taniguchi, H. Yamaji, Y. Maeda, K. Toyohara, K. Miyamoto, Y. Kimura, K. Oda, *Science* **2016**, *351*, 1196.
- [17] Z. Zhou, R. Song, J. Xu, X. Ni, Z. Dang, Z. Zhao, J. Quan, S. Dong, W. Hu, D. Huang, K. Chen, Z. Wang, X. Cheng, M. B. Raschke, A. Alù, T. Jiang, *Nano Lett.* **2023**, *23*, 11252.
- [18] K. Lempicka-Mirek, M. Król, H. Sigurdsson, A. Wincukiewicz, P. Morawiak, R. Mazur, M. Muszynski, W. Piecek, P. Kula, T. Stefaniuk, M. Kaminska, L. De Marco, P. G. Lagoudakis, D. Ballarini, D. Sanvitto, J. Szczytko, B. Pietka, *Sci. Adv.* **2022**, *8*, eabq7533.
- [19] Y. Koo, T. Moon, M. Kang, H. Joo, C. Lee, H. Lee, V. Kravtsov, K.-D. Park, *Light: Sci. Appl.* **2024**, *13*, 30.
- [20] R. Hertwig, S. Nishiwaki, A. N. Tiwari, R. Carron, *Solar RRL* **2022**, *6*, 2200268.
- [21] J. A. Hutchison, T. Schwartz, C. Genet, E. Devaux, T. W. Ebbesen, *Angew. Chem., Int. Ed.* **2012**, *51*, 1592.
- [22] M. Hertzog, M. Wang, J. Mony, K. Börjesson, *Chem. Soc. Rev.* **2019**, *48*, 937.
- [23] D. O. Dorohoi, M. Postolache, C. D. Nechifor, D. G. Dimitriu, R. M. Albu, I. Stoica, A. I. Barzic, *Molecules* **2023**, *28*, 2955.
- [24] A. Shalabney, J. George, H. Hiura, J. A. Hutchison, C. Genet, P. Hellwig, T. W. Ebbesen, *Angew. Chem. Int. Ed. Engl.* **2015**, *54*, 7971.
- [25] K. S. Menghrajani, M. Chen, K. Dholakia, W. L. Barnes, *Adv. Opt. Mater.* **2022**, *10*, 2102065.
- [26] W. M. Takele, L. Piatkowski, F. Wackenhut, S. Gawinkowski, A. J. Meixner, J. Waluk, *Phys. Chem. Chem. Phys.* **2021**, *23*, 16837.
- [27] E. Rebollar, S. Pérez, M. Hernández, C. Domingo, M. Martín, T. A. Ezquerra, J. P. García-Ruiz, M. Castillejo, *Phys. Chem. Chem. Phys.* **2014**, *16*, 17551.
- [28] S. Mahajan, R. M. Cole, J. D. Speed, S. H. Pelfrey, A. E. Russell, P. N. Bartlett, S. M. Barnett, J. J. Baumberg, *J. Phys. Chem. C* **2010**, *114*, 7242.
- [29] A. Balčytis, T. Tolenis, X. Wang, G. Seniutinas, R. Drazdys, P. R. Stoddart, S. Juodkaziš, *arXiv* **2016**, 08197.
- [30] Y. Nishikawa, T. Nagasawa, K. Fujiwara, M. Osawa, *Vib. Spectrosc.* **1993**, *6*, 43.
- [31] S. Foteinopoulou, G. C. R. Devarapu, G. S. Subramania, S. Krishna, D. Wasserman, *Nanophotonics* **2019**, *8*, 2129.
- [32] A. Sau, K. Nagarajan, B. Patraha, L. Lethuillier-Karl, R. M. A. Vergauwe, A. Thomas, J. Moran, C. Genet, T. W. Ebbesen, *Angew. Chem., Int. Ed.* **2021**, *60*, 5712.
- [33] A. Thomas, J. George, A. Shalabney, M. Dryzhakov, S. J. Varma, J. Moran, T. Chervy, X. Zhong, E. Devaux, C. Genet, J. A. Hutchison, T. W. Ebbesen, *Angew. Chem., Int. Ed.* **2016**, *55*, 11462.
- [34] K. Hirai, H. Ishikawa, T. Chervy, J. A. Hutchison, H. Uji-i, *Chem. Sci.* **2021**, *12*, 11986.
- [35] M. V. Imperatore, J. B. Asbury, N. C. Giebink, *J. Chem. Phys.* **2021**, *154*, 191103.
- [36] S. L. Zhang, J. C. M. Li, *J. Polym. Sci., Part B: Polym. Phys.* **2004**, *42*, 260.
- [37] M. S. Rider, R. Arul, J. J. Baumberg, W. L. Barnes, *Nanophotonics* **2022**, *11*, 3695.
- [38] S. Babar, J. H. Weaver, *Appl. Opt.* **2015**, *54*, 477.
- [39] X. Zhang, J. Qiu, J. Zhao, X. Li, L. Liu, *J. Quant. Spectrosc. Radiat. Transfer* **2020**, *252*, 107063.